THE UNIVERSITY of EDINBURGH

Edinburgh Research Explorer

The VLT Survey Telescope ATLAS

Citation for published version:
Shanks, T, Metcalfe, N, Chehade, B, Findlay, JR, Irwin, MJ, Gonzalez-Solares, E, Lewis, JR, Yoldas, AK, Mann, RG, Read, MA, Sutorius, ETW & Voutsinas, S 2015, 'The VLT Survey Telescope ATLAS', *Monthly Notices of the Royal Astronomical Society*, vol. 451, no. 4, pp. 4238-4252.
https://doi.org/10.1093/mnras/stv1130

Digital Object Identifier (DOI):
10.1093/mnras/stv1130

Link:
Link to publication record in Edinburgh Research Explorer

Document Version:
Early version, also known as pre-print

Published In:
Monthly Notices of the Royal Astronomical Society

General rights
Copyright for the publications made accessible via the Edinburgh Research Explorer is retained by the author(s) and / or other copyright owners and it is a condition of accessing these publications that users recognise and abide by the legal requirements associated with these rights.

Take down policy
The University of Edinburgh has made every reasonable effort to ensure that Edinburgh Research Explorer content complies with UK legislation. If you believe that the public display of this file breaches copyright please contact openaccess@ed.ac.uk providing details, and we will remove access to the work immediately and investigate your claim.

Download date: 27. Jul. 2024

Mon. Not. R. Astron. Soc. **000**, ??–?? (0000) Printed 20 February 2015 (MN LATEX style file v2.2)

The VLT Survey Telescope ATLAS

T. Shanks[1⋆], N. Metcalfe[1], B. Chehade[1], J.R. Findlay[1], M.J. Irwin[2], E. Gonzalez-Solares[2], J.R. Lewis[2], A. Kupcu Yoldas[2], R.G.Mann[3], M.A. Read[3], E.T.W. Sutorius[3], S. Voutsinas[3]
[1]*Physics Department, University of Durham, South Road, Durham, DH1 3LE, UK*
[2]*Institute of Astronomy, Univ. of Cambridge, Madingley Road, Cambridge, CB3 0HA, UK*
[3]*Institute for Astronomy, Univ. of Edinburgh, Blackford Hill, Edinburgh EH9 3HJ, UK.*

arXiv:1502.05432v1 [astro-ph.GA] 18 Feb 2015

20 February 2015

ABSTRACT

The VLT Survey Telescope (VST) ATLAS is an optical *ugriz* survey aiming to cover ≈ 4700deg^2 of the Southern sky to similar depths as the Sloan Digital Sky Survey (SDSS). From reduced images and object catalogues provided by the Cambridge Astronomical Surveys Unit we first find that the median seeing ranges from $0.''8$ FWHM in i to $1.''0$ in u, significantly better than the $1.''2 - 1.''5$ seeing for SDSS. The 5σ magnitude limit for stellar sources is $r_{AB} = 22.7$ and in all bands these limits are at least as faint as SDSS. SDSS and ATLAS are more equivalent for galaxy photometry except in the z band where ATLAS has significantly higher throughput. We have improved the original ESO magnitude zeropoints by comparing $m < 16$ star magnitudes with APASS in *gri*, also extrapolating into u and z, resulting in zeropoints accurate to $\approx \pm 0.02$mag. We finally compare star and galaxy number counts in a 250deg^2 area with SDSS and other count data and find good agreement. ATLAS data products can be retrieved from the ESO Science Archive, while support for survey science analyses is provided by the OmegaCAM Science Archive (OSA), operated by the Wide-Field Astronomy Unit in Edinburgh.

Key words: cosmology: observations, large-scale structure, astronomical data bases: surveys.

1 INTRODUCTION

The ATLAS survey (Shanks et al. 2013) is carried out on the VLT Survey Telescope (VST), a 2.61-m telescope situated at Cerro Paranal Observatory (Schipani et al. 2012). It uses the OmegaCAM camera(Kuijken et al 2011) containing 32 4k×2k CCDs with a total of 268 megapixels. The field-of-view of the camera is 1×1deg^2 and the pixel size is 0.21arcsec. The aim of the survey is to produce a *ugriz* catalogue to the equivalent depth of SDSS but in the Southern Hemisphere, with a target area of ≈ 4700deg^2. Although the survey was only specified to have seeing in the range $1 - 1.''4$ FWHM, with the better seeing going to the VST KiDS survey (de Jong et al. 2013), ATLAS is proving to have better median seeing than expected, at the subarcsecond level. The survey is being made alongside its sister VISTA Hemisphere Survey (VHS, McMahon et al. 2013) which is supplying YJK. The survey depths are also well matched to the WISE survey (Wright et al. 2010) at the mid-IR L and M bands. The footprint of the survey is shown in Fig. 1 where it is compared to the footprints of KiDS and VHS. The deeper VISTA VIKING NIR survey (Edge et al. 2013) has approximately the same footprint as KiDS. ATLAS has yearly data releases with DR1 occurring in April 2013 and covering ≈ 1500deg^2 of data taken before 30/9/12 and DR2 now imminent and covering ≈ 2500deg^2 taken before 30/9/13.

1.1 ATLAS Science Aims

The primary aims of the ATLAS survey are cosmological. The UV sensitivity of the survey gives it an advantage in terms of quasar surveys that in the Southern Hemisphere can be followed up using instruments like AAT 2dF or VISTA 4MOST. These surveys can then be used, for example, to look for any evidence of excess power in the quasar clustering data that might provide evidence for primordial non-Gaussianity in the early Universe. It may also be possible to search for BAO at the 100Mpc scale in the unexplored $0.8 < z < 2.2$ redshift range. These analyses can be done ei-

⋆ E-mail: tom.shanks@durham.ac.uk

ther by photo-z using selection codes like XDQSO-Z (Bovy et al. 2012) or by using spectroscopic redshifts. We have already used AAT 2dF to make a redshift survey of ≈ 10000 quasars using UVX and NIR selection and these are being used to study the luminosity and clustering correlation function of dusty and unobscured quasars (Chehade et al 2014 in prep.). This quasar redshift survey can also form the base for photo-z clustering analyses over the whole VST ATLAS area. Such quasar surveys will also complement future programmes such as the X-ray AGN surveys of e-ROSITA (Merloni et al. 2012).

Another cosmological aim is to test for the ISW effect by cross-correlating the 2-D positions of Luminous Red Galaxies with microwave background temperature fluctuations e.g. (Sawangwit et al. 2010). This is one of the few independent tests of the accelerating expansion of the Universe and the Southern Hemisphere is the only place left to improve the statistical significance of this test.

The galaxy and quasar surveys can also be combined to study the quasar lensing magnification bias at high redshift and the quasar galaxy clustering environment at low redshifts (e.g. Mountrichas & Shanks 2007). ATLAS will also take advantage of its excellent seeing to allow many galaxy lensing shear projects. Although not as deep as KiDS, ATLAS shares the same VST platform which means that the advantages of low optical distortion are shared by ATLAS for lensing projects.

We shall also be looking at galaxy counts and how they vary over the sky at bright magnitudes. Previous observations from 2MASS have suggested that there exists a galaxy under-density in the Southern Hemisphere (Keenan, Barger, & Cowie 2013; Whitbourn & Shanks 2014) and we wish to test for the existence of this 'Local Hole' at optical wavelengths. Since VST ATLAS will also cover the Great Attractor region, this means that it can use the form of bright galaxy counts to search a large area in this direction for clusters and superclusters even behind Shapley 8.

Mapping the Southern Hemisphere using galaxy clusters is also another cosmological aim of VST ATLAS. The *riz* bands will be combined with VHS and WISE NIR bands to select galaxy clusters to $z \approx 1$.

There are many other non-cosmological projects that can be done with ATLAS. The discovery of dwarf satellite galaxies and stellar streams in the Southern Hemisphere is one clear example (Belokurov et al. 2014; Koposov et al. 2014) and ATLAS is also being used to search for high redshift quasars via the Lyman-break technique (Carnall et al, 2014a, in prep.)

2 ATLAS DESCRIPTION

2.1 Survey area

As can be seen from Fig. 1, the ATLAS South Galactic Cap area (SGC) area lies between 21h30 <RA < 04h00 and −40 < Dec < −10. The NGC area lies between 10h00<RA <15h30 and −20 < Dec < −2.5 plus 10h00 < RA < 15h00 and -30 <Dec < -20. The total area of the survey is 4711 deg^2 with 2087 deg^2 in the NGC and 2624 deg^2 in the SGC. The NGC area below Dec<-20 is so far approved in *iz* and is the subject of a Chilean ESO proposal in *ugr*. There is also an ongoing 'Chilean *u* extension project' to double the exposure time in *u* from 2 mins to 4 mins over the full ATLAS area (PI L. Infante). Status maps of the ATLAS survey can be found at `http://astro.dur.ac.uk/Cosmology/vstatlas/`.

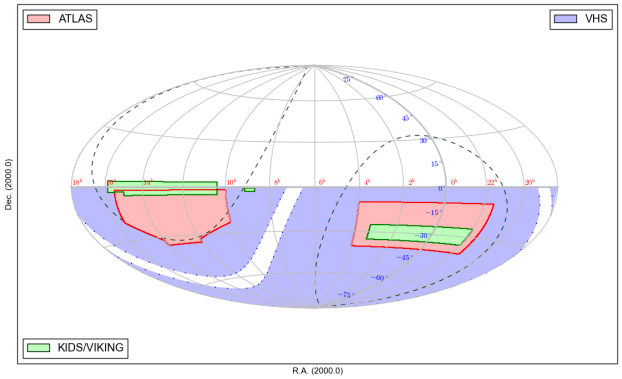

Figure 1. ATLAS footprint (red) compared to VHS (purple) and KIDS(green). VHS surveys the whole hemisphere except at ±5 deg. from the Galactic plane.

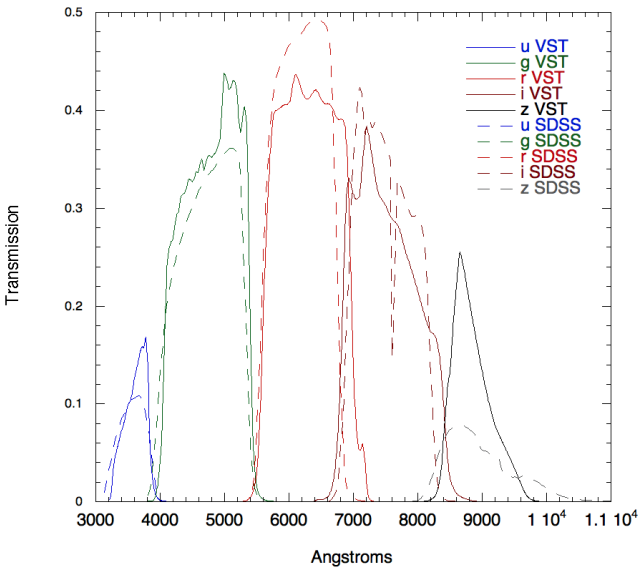

Figure 2. ATLAS and SDSS filter + telescope + atmospheric transmissions compared. All are calculated at airmass 1.3. No Atmospheric Dispersion Corrector is assumed for the ATLAS filters since it is not being used.

2.2 Survey observations

OmegaCAM camera pixels are 0.213×0.213arcsec^2 in size so approximately half the dimensions of 0.396×0.396arcsec^2 SDSS pixels. The *ugriz* band transmissions are shown in Fig. 2 where they are compared to those for SDSS. They are seen to be similar in all bands except for *z* where ATLAS has an ≈ 2× higher throughput. The ATLAS exposure times have been conservatively increased over the typical SDSS 54s exposure to maintain the S/N achieved by SDSS taking into account increased read-out noise and, potentially, sky brightness, particularly in *i* and *z* (see Table 1). The OmegaCAM read-out noise is typically 5-6 electrons per pixel and

Band	u	g	r	i	z
Exposure	2×60s	2×50s	2×45s	2×45s	2×45s
Seeing	$1.''02$	$0.''95$	$0.''90$	$0.''81$	$0.''84$
SDSS Seeing	$1.''46$	$1.''36$	$1.''24$	$1.''18$	$1.''20$
Mag Lim	21.99	23.14	22.67	21.99	20.87
Mag Lim (gal)	21.78	22.71	22.17	21.40	20.23
SDSS Mag Lim	21.87	22.75	22.31	21.71	20.17
Sky Brightness	22.34	21.90	20.92	19.78	18.85
SDSS Sky Bri.	22.15	21.85	20.86	20.20	19.00
$20^m\ e^-/s$	29	177	160	101	29
SDSS $20^m\ e^-/s$	33	175	174	116	19

Table 1. ATLAS basic characteristics. ATLAS median seeing for ESO A,B classified tiles. SDSS median seeing is taken from Bramich & Freudling (2012). Mag Lim (ATLAS) corresponds to the median 5σ magnitude detection limit for stars as measured in a $1''$ radius aperture. Mag Lim (gal) corresponds to ATLAS 5σ limit now calculated in apertures of the SDSS seeing radius at airmass 1.0. SDSS Mag Lim corresponds to 5σ SDSS point source detection limits based on the above fluxes and calculated in a radius of the above median SDSS seeing at airmass 1.0. Sky brightness is measured in mag/arcsec^2. SDSS DR1 sky brightness is median of 77068 frames from `http://www.sdss2.org/dr7/products/general/seeing.html`. Fluxes are given at 20^m for ATLAS and SDSS normalised to airmass 1.3. SDSS fluxes come from Stoughton et al. (2002) eqn. (1). All magnitudes are quoted in the AB system.

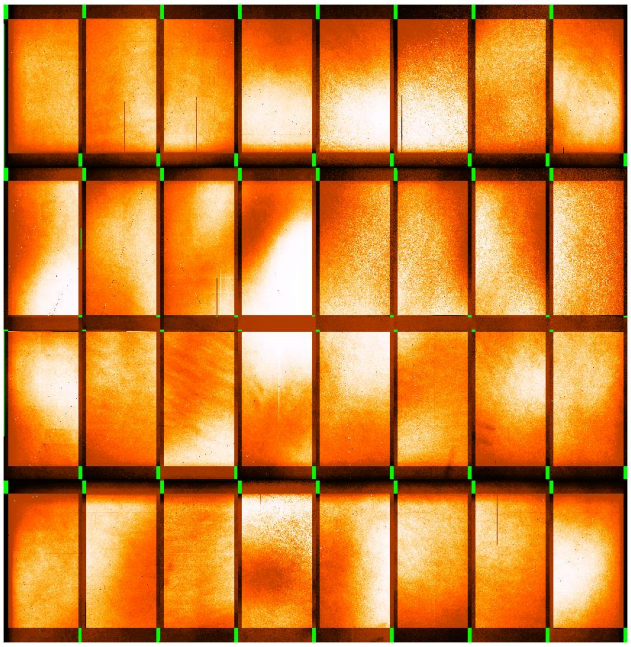

Figure 3. Typical ATLAS confidence map for a stacked tile in r. Areas left uncovered by the 2-pawprint dither are shown in green. Those at the perimeter of the tile area will be covered by the $2'$ tile overlaps.

the gain is ≈ 2.2 with 10% chip-to-chip RMS. Double exposures are taken, dithered by $85''$ in Declination and $25''$ in RA, to cover the main inter-chip gaps ($80.''5$ and $11.''8$ in Declination and $21.''5$ in RA) and to allow cosmic rays to be rejected. The 2-pointing dither and $2'$ tile overlaps leaves 28 ($80.''5 \times 21.''5$) and 14 ($11.''8 \times 21.''5$) small holes (see green areas in Fig. 3) amounting to $\approx 1/3$% of the total area. Each OmegaCAM field is $\approx 1 \times 1$deg^2 and each tile has a $58'$ centre-to-centre spacing, giving a $\approx 2'$ overlap between tiles in both the RA and Dec directions.

For each VST ATLAS tile, 2 dithered exposures in each of the *ugr* bands were observed in dark time and 2 dithered exposures in each of the *iz* bands in grey/bright time. For all except the first 2 months of the survey, the observations were done in concatenations of 17 fields which approximately filled a 1hr ESO Observing Block (OB) in u (including overheads) and slightly less in the other bands. The seeing is specified to be $< 1.''4$ FWHM.

The imaging data has been reduced by CASU using the VST data flow software. The images were trimmed and debiased using nightly calibration frames and then flat-fielded using accumulated monthly stacked twilight sky flats. The frames are then corrected for crosstalk and defringed if necessary. The sub-exposures are then automatically registered and stacked. The resulting imaging data comprises the combination of the two individual images for each of the original CCDs. Each file is in a multi-extension fits (MEF) format with an extension for each of the 32 OmegaCam CCDs in the stacked tile. Individual CCDs originally contained 2048×4096 pixels and the stacked pawprint extensions contain $\approx 2165 \times 4498$ pixels to cover the two $25'' \times 85''$ offset CCDs that make up each extension in a stack. This leaves $\approx 5''$ overlaps between the stacked pawprints in each direction where objects can be recorded twice. Along with the imaging data, statistical confidence maps in the same format are also supplied (Irwin et al. 2004). In Fig. 3 we show a typical confidence map from the r band. The main 'bar-like' pattern seen is due to the interchip gaps and the dither pattern used to cover them. Note that these are detector-level normalised confidence maps whereby each detector's map is normalised to a median level of 100%, hence the particular shape of the repeating pattern.

Object detection is then carried out to an isophotal limit set to 1.25σ where σ is a robust (rms) estimate of the average pixel noise over the frame. Catalogues are then produced for the stacked and unstacked images. Aperture, Petrosian and Kron magnitudes are supplied in the first instance along with many other parameters (see Section 2.6 below).

2.3 Astrometry

Astrometric calibration is via the numerous unsaturated 2MASS point sources available in each field. By stacking residuals from a series of standard Tangent Plane astrometric fits based on 2MASS we can see (as in the example in Fig. 4) that there are no significant astrometric distortions over the whole field of view. The individual detector astrometric solutions achieve rms accuracies of around 70-80mas per star - generally dominated by rms errors in 2MASS stars. Even at high Galactic latitudes there are sufficient calibrators to give systematic residuals at the 25mas level per detector. The global systematics from stacking multiple solutions are better than this as can be seen in Fig. 4. A Tangent Plane projection (TAN) is being used for all data products.

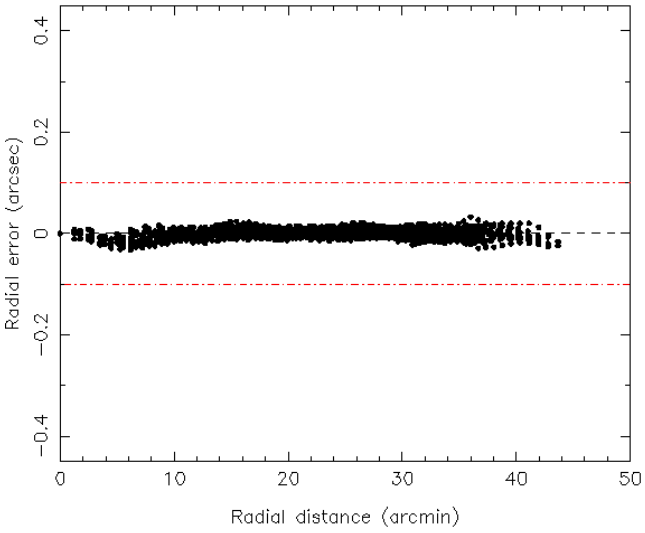

Figure 4. ATLAS astrometric accuracy from 2MASS comparison. The red dashed lines represent reference levels of ±100mas astrometric accuracy.

2.4 Illumination correction

The open nature of the VST dome provides excellent through-flow of air improving the seeing by reducing the contribution from the dome. However, this also leads to increased scattered light which impairs flat-fielding. In particular a ≈ 0.2mag centre to the edge gradient in the photometry is seen from the pawprint. An illumination correction therefore has to be applied to the photometry and this has been done via the AAVSO Photometric All-Sky Survey (APASS) survey (`http://www.aavso.org/apass`). The APASS survey is a $g < 16$mag stellar survey made in the $BVgri$ bands. The illumination corrections are obtained from direct, stacked, comparisons between ATLAS and APASS stelar magnitudes for gri and from extrapolating APASS gri to provide the u and z corrections. The pattern of residuals across the tile typically looks like that shown in Fig. 5. The scattered light is made up of multiple components having different symmetries and scales causing effects ranging in scale from ten arcseconds with $x-y$ rectangular symmetry, e.g. due to scattering off masking strips of CCDs, to large fractions of the field due to radial concentration in the optics and to non-astronomical scattered light entering obliquely in flats. The illumination correction removes the dominant reproducible components of this effect in the source lists leaving the zeropoint across the field uniform to ≈ ±0.007mag. The illumination correction is updated on a few months timescale as necessary.

We can test the illumination corrections in the overlap area with SDSS. Fig. 6 shows SDSS-ATLAS residuals from a stack of 10 ATLAS i-band tiles in the overlap area. The amplitude of the radial pattern of residuals is much reduced from that shown in Fig. 5.

2.5 ATLAS zeropoint calibration

The original zeropoint calibration was based on the ESO nightly standards in all bands and these were used to place the VST magnitudes for each tile on a Vega-like system.

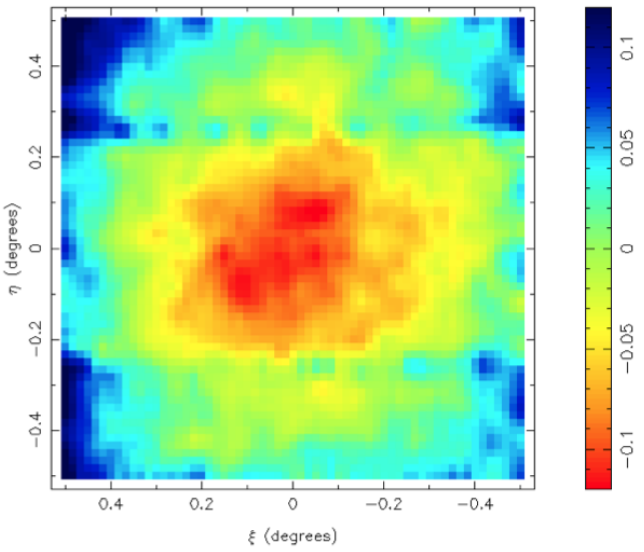

Figure 5. ATLAS illumination correction. ATLAS i-band observations processed using the same master flats for the period 16/8-30/9/12 and the resulting residuals from the 2MASS photometric catalogue stacked over several hundred independent pointings. The i-band colour equations are $i = J + (J-K) * 1.175 + 0.459$ (for $H - K \leqslant 0.15$) and $i = J + (J-K) * 1.175 + 0.459 + (H - K - 0.15) * 3.529$ (for $H - K > 0.15$).

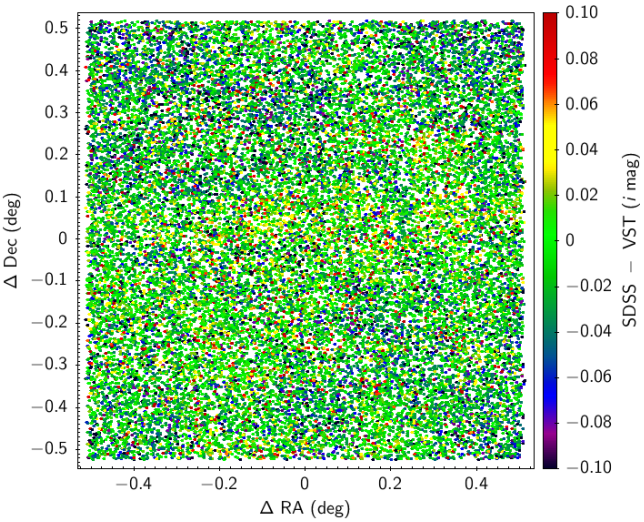

Figure 6. SDSS-ATLAS stellar residuals in i from a 10-field stack after ATLAS illumination correction.

These standards are observed in any photometric conditions and so cloud can introduce zeropoint error. However, due to the excellence of the Paranal site and the clear conditions specified for ATLAS observations, there appears to be a reasonable consistency between the zeropoints in night-to-night comparisons. So these ESO standard zeropoints make a good first-order calibration of the survey. But in making stellar colour-colour diagrams Chehade et al (2014 in prep.) found that the stellar locus moved on a regular basis, presumably due to non-photometric conditions in one of the bands between survey field and standard star. Therefore there is a need for an improved global calibration for ATLAS and we

have thus made a first iteration towards a global calibration via APASS.

We used APASS to produce new magnitude zeropoints based on a tile-by-tile comparison of unsaturated $g < 16$ mag stars in each ATLAS *gri* tile. In the u and z bands where there is no APASS data, we again extrapolated from the APASS *gri* bands band to produce the u and z calibrations. In APASS, the average star sky density is $\approx 100\mathrm{deg}^{-2}$ although at high latitudes, the star density may be lower. Therefore to improve the statistics we have also implemented a nightly ATLAS zeropoint based on all the APASS standards observed that night. This also has the effect of averaging out any APASS systematic in an individual ATLAS field. We now assume the nightly zeropoint as our default calibration. This calibration can be checked in the SDSS sub-areas and we will report on the results of this check in Section 4.2.

Note that despite the fact that the original ESO zeropoints are in the Vega magnitude system, APASS uses the AB system and so the default for this paper is that the magnitudes are on the APASS AB system unless explicitly stated otherwise. The AB-Vega magnitude offsets were computed to be 0.894 (u), -0.100 (g), 0.159 (r), 0.356 (i), 0.517 (z). These were calculated for VST telescope and filter throughput and at airmass 1.3 (see Fig. 2) for consistency with SDSS conversions.

We then compared APASS nightly magnitude zeropoints with the original ESO zeropoints. Fig 7 shows distributions of APASS-ATLAS magnitude zeropoint differences on a field-by-field basis over the whole current survey area. We find that the residuals are basically at the $\pm$0.05mag level but with non-Gaussian tails usually arising from non-photometric conditions. From Fig. 7 we also note that the APASS-ESO offsets are in good agreement with the expected offsets except in the case of u which has a 0.3mag discrepancy. It is probable that the u band fabricated from APASS *gri* contains a zeropoint error and this is confirmed in the comparison with SDSS made in Section 3.2 below. This problem will be corrected at the global calibration stage (Findlay et al 2015, in prep).

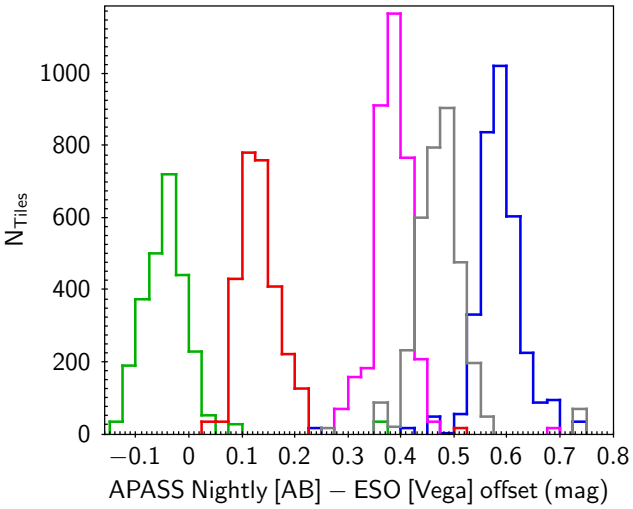

Figure 7. APASS nightly-ESO ATLAS magnitude zeropoint offsets on a tile-by-tile basis over the whole current survey for u (blue), g (green), r (red), i (purple), z (grey). Here APASS is in AB whereas ESO ATLAS is in the Vega system. The average APASS-ESO magnitude offsets and standard deviations are 0.59 ± 0.06 (u), -0.042 ± 0.06 (g), 0.13 ± 0.045 (r), 0.39 ± 0.038 (i), 0.47 ± 0.080 (z).

2.6 ATLAS photometric parameters

The photometric quantities supplied for ATLAS are Kron and Petrosian pseudo-total magnitudes along with their respective radii. Kron and Petrosian magnitudes are measured in these radii multiplied by a factor of 2×. Aperture magnitudes are also given with radii of $1/2\times r_{core}$, $1/\mathrm{sqrt}(2)\times r_{core}$, r_{core}, $\mathrm{sqrt}(2)\times r_{core}$, $2\times r_{core}$, $2\mathrm{sqrt}(2)\times r_{core}$, $4\times r_{core}$, $5\times r_{core}$, $6\times r_{core}$, $7\times r_{core}$ where $r_{core} = 1''$ and is the radius of aperture 3. Corrections to total magnitudes for the aperture magnitudes of point sources are also supplied. The Kron, Petrosian and aperture magnitudes for both point sources and extended objects are deblended of overlapping sources. Areal profiles are given as the number of pixels above 8 thresholds. Star-galaxy separation statistics, peak heights, sky levels and sky variance are also calculated. A number of other parameters are given and a full list is available at `http://casu.ast.cam.ac.uk/surveys-projects/vst/technical/catalogue-generation`

2.7 Survey statistics

The seeing distributions by passband are shown in Fig. 8. These show that the median seeing from the CASU measurements is subarcsecond in the *riz* bands, and even at *ug* only rises to $\approx 1''$ FWHM. The individual median seeings in each band are given in Table 1. These are significant improvements over median SDSS seeing values e.g. $1.''24$ FWHM in r (Bramich & Freudling 2012). The distribution of limiting magnitudes at the 5σ detection level by passband is shown in Fig. 9. The median 5σ stellar magnitude limit in a $1''$ radius aperture reaches $r \approx 22.7$. The median limits in all bands are also given in Table 1. Also given there are ATLAS median magnitude limits calculated in apertures of radius the SDSS FWHM seeing and these might be thought more comparable to faint galaxy S/N limits. In Fig. 10 we similarly show the distribution of sky brightnesses and the medians are again given in Table 1. Finally, in Table 1, we also present the count rate in each ATLAS passband for a 20^m (AB) point source based on the magnitude zeropoints.

In Table 1 we also present SDSS statistics for comparison, including seeing, sky brightness and count rates. SDSS seeing statistics are taken from Bramich & Freudling (2012) and sky brightness statistics are sourced from `http://www.sdss2.org/dr7/`. As already noted, in all bands median ATLAS seeing is significantly better than that of SDSS. Comparing SDSS and ATLAS median sky brightnesses we note that the ATLAS sky brightnesses are fainter than SDSS in u, g, r and slightly brighter in i and z due to ATLAS using grayer conditions for i, z. The SDSS count rates are also given from Stoughton et al. (2002) eqn. (1) assuming airmass 1.3, as are the quoted ATLAS count rates. We see that the ATLAS and SDSS count rates are similar with ATLAS having a significant advantage only at z, the same conclusion as from the throughput comparison in Fig. 2. The SDSS magnitude limits have been calculated assuming these

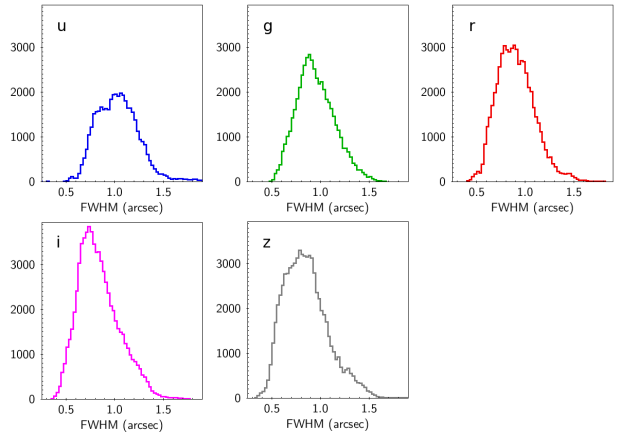

Figure 8. ATLAS FWHM seeing distributions in arcseconds. These are for ESO A and B grade tiles.

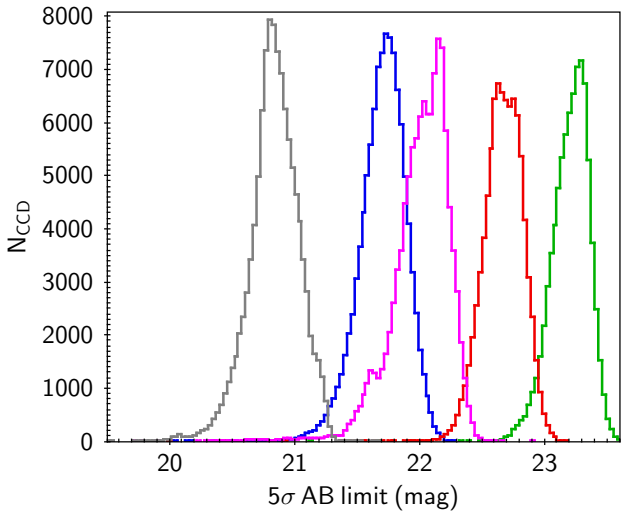

Figure 9. ATLAS 5σ AB magnitude limit distributions for point sources in u (blue), g (green), r (red), i (purple) and z (grey). The median magnitude limits are given in Table 1 where they are compared to the equivalent SDSS limits.

SDSS count rates and sky brightnesses. They are again 5σ limits for point sources but now measured in the radius of the quoted SDSS seeing (ie $\theta < 1.''46$ in u). This means that the ATLAS limits are $\approx 0.^m25$ fainter in $ugri$ due to better seeing and $0.^m7$ fainter in z, with this extra advantage due to ATLAS' higher throughput in the z band. The comparison of these limits is more favourable to SDSS when the bigger apertures are used to compute ATLAS 5σ limits (Mag Lim (gal)). These are more like the apertures appropriate for faint ATLAS galaxies. Here ATLAS is within 0.15mag of the SDSS limit in $ugrz$ but ATLAS has a $0.^m31$ disadvantage in i partly due to a brighter sky brightness. Note that ATLAS is sky noise limited in $griz$ and read-out-noise limited in u. We conclude that SDSS and ATLAS appear to have comparable magnitude limits for galaxy photometry but that ATLAS has significantly fainter limits than SDSS for stellar photometry mainly due to its better seeing.

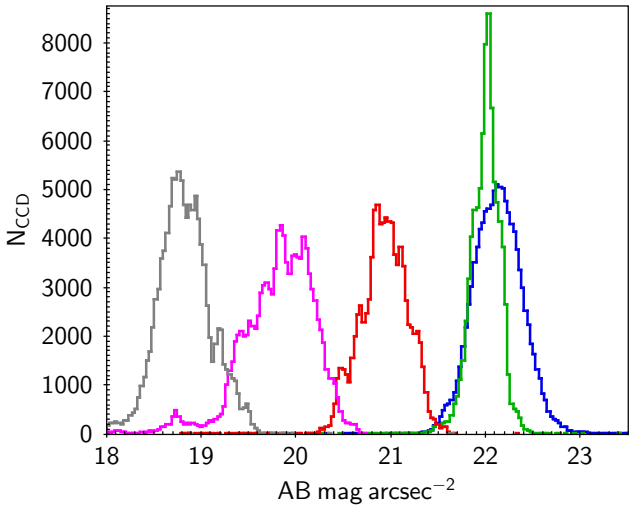

Figure 10. ATLAS sky brightness distributions in u (blue), g (green), r (red), i (purple) and z (grey). The median sky brightnesses are given in Table 1 where they are compared to their SDSS equivalents.

3 PHOTOMETRIC SCALES AND COLOUR EQUATIONS

3.1 ATLAS-Vega colour equations

As noted above, the original photometric calibration (as used in ATLAS DR1) was based on the limited number of standard fields observed on most nights. This 'ESO' calibration is in a VST Vega-like system and remains available as an alternative calibration, despite the known issue with occasional non-photometric conditions. Nevertheless, we list below the linear colour equations used to convert the standards to an internal VST system for the ESO Vega calibration :

$$u_{vst} = U + 0.035(U - B)$$

$$g_{vst} = B - 0.405(B - V)$$

$$r_{vst} = R + 0.255(V - R)$$

$$i_{vst} = I + 0.115(R - I)$$

$$z_{vst} = I - 0.390(R - I)$$

As noted in Section 2.5, we have since re-calculated all the zero-points based now on the illumination-correction fixed catalogues while computing APASS AB nightly and field-by-field magnitude zero-points.

3.2 ATLAS-SDSS colour equations

In the equatorial regions there is a $\approx 300\text{deg}^2$ overlap with SDSS, split between the SGC ($\approx 180\text{deg}^2$) and the NGC ($\approx 120\text{deg}^2$). In the SGC the overlap is at RA$\approx$22h40-03h, $-11 < Dec < -9$ and in the NGC it is at RA$\approx$10h00-15h30,$-3.5 < Dec < -2$deg. We have compared $ugriz$ (AB) colours of SDSS and ATLAS stars in the 120deg^2 NGC overlap region to define the colour equations between the two

systems. We use PSF magnitudes for SDSS and aperture 3 (corrected to total) magnitudes for ATLAS. The magnitude ranges used are $14 < u < 20$, $15 < g < 20$, $15 < r < 20$, $14 < i < 19$ and $13.5 < z < 18.5$.

In Fig. 11 we show $u_{SDSS} - u : u - g$, $g_{SDSS} - g : g - r$, $r_{SDSS} - r : g - r$, $i_{SDSS} - i : r - i$, $z_{SDSS} - z : i - z$. We see that the colour terms in u and i are almost negligible but there are small colour terms in grz. We find that:

$$u_{SDSS} = u_{VST} + 0.01(u-g)_{SDSS} + 0.27$$

$$g_{SDSS} = g_{VST} + 0.05(g-r)_{SDSS} - 0.06$$

$$r_{SDSS} = r_{VST} + 0.03(g-r)_{SDSS} - 0.035$$

$$i_{SDSS} = i_{VST} - 0.025$$

$$z_{SDSS} = z_{VST} - 0.04(i-z)_{SDSS} + 0.04$$

We note that the zeropoint offsets with SDSS are small and due to slight differences in effective bandpass wavelengths. The exception is u where the APASS AB zeropoints had to be fabricated from APASS gri. This is due to the non-linear (even double-valued for some star types) transformation really required when going from g, r to u. We have investigated if these offsets are caused by the method of magnitude measurement and find that these results are robust. Note that this issue in u does not affect the AB magnitudes in Table 1 and Figs. 7, 9 and 10 since these are based on the original ESO Vega calibration plus the computed AB-Vega offsets given in Section 2.5.

We find good agreement in the colour coefficients with the SDSS-VST gri band conversions independently reported by the KiDS team at `http://kids.strw.leidenuniv.nl/DR1/images/cterms.png` as

$$g_{SDSS} = g_{VST} + 0.0522(g-r)_{SDSS}$$

$$r_{SDSS} = r_{VST} + 0.0321(g-r)_{SDSS}$$

$$i_{SDSS} = i_{VST} + 0.0155(r-i)_{SDSS}$$

Typical extinction coefficients (mags) for ATLAS are $0.46(u)$, $0.19(g)$, $0.09(r)$, $0.05(i)$, $0.05(z)$.

3.3 ATLAS-SDSS comparison

We next compare linearity of the ATLAS photometry (calibrated via nightly APASS and after the above colour corrections), with SDSS in the $\approx 120\text{deg}^2$ NGC overlap area. We shall see later that there are still some area-dependent zeropoint problems with the nightly APASS calibrations but here we will focus on the r-band where the field-field problems are less. In the top panel of Fig. 12 we plot ATLAS aperture magnitudes versus model magnitudes for SDSS stars. The relation is consistent with linearity over the full $13 < r < 22.5$ mag range. In the middle panel of Fig. 12 we plot ATLAS Kron magnitudes against SDSS model magnitudes for galaxies. An offset to total of -0.15mag for galaxies is suggested for ATLAS. The relation appears noisier than the stars as expected but with no evidence of a scale error to

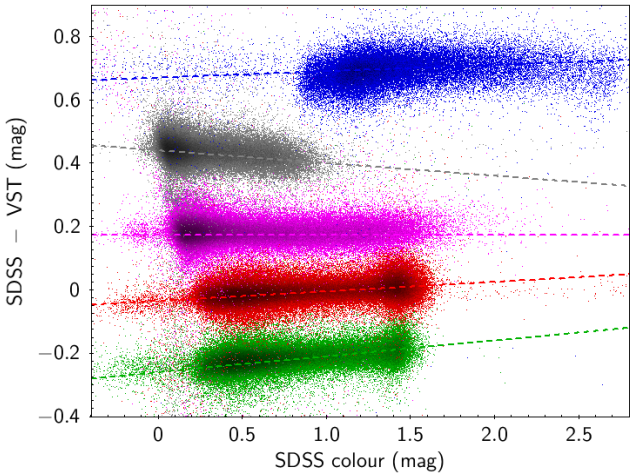

Figure 11. Colour equations between ATLAS aperture 3 AB magnitudes and SDSS PSF magnitudes for stars in u (blue), g (green), r (red), i (purple) and z (grey). Here the ATLAS AB magnitudes are derived from the APASS nightly zeropoints. The points have been displaced in the ordinate for clarity, $g_{SDSS} - g$ by -0.2, $i_{SDSS} - i$ by +0.2, $z_{SDSS} - z$ by +0.4 and $u_{SDSS} - u$ by +0.4. Apart from this, the dashed lines are the equations given in Sect:3.2.

$r \approx 22$. In the bottom panel of Fig. 12 we similarly plot ATLAS Petrosian magnitudes for galaxies against model magnitudes for SDSS. We see a reasonably linear, if noisier, relation. In the $22 < r < 22.5$ bin the rms error reaches ± 0.2, ± 0.38 and ± 0.38 mag for aperture, Petrosian and Kron magnitudes and here we might expect roughly equal contributions from ATLAS and SDSS. Overall, for VST ATLAS, we therefore recommend that aperture magnitudes (aper_3) are used for stars while Petrosian or Kron magnitudes are used for galaxies.

These results for the r band are typical of the results for the other 4 bands. These can be found at `http://astro.dur.ac.uk/Cosmology/vstatlas/tests/`.

3.4 ATLAS-Stripe 82 (WHDF field) comparison

Because SDSS only reaches a similar depth to ATLAS, it is not clear which survey is dominating the error spread at faint magnitudes. We have therefore also compared ATLAS photometry for galaxies and stars with the much deeper Stripe 82 (S82) photometry which lies within a 1deg^2, specially observed, ATLAS area which also contains the William Herschel Deep Field (Metcalfe et al 2005) and again its deeper multi-epoch photometry allows a comparison to check the magnitude dependent error of the ATLAS photometry.

We note that although the WHDF ATLAS data has the same exposure as the ATLAS survey data and was taken in dark time, the seeing particularly in u and g is significantly worse than average (see Table 2). Indeed, the 5σ point source magnitude limits in all bands are brighter than the ATLAS average from ≈ 0.2mag in riz, to 0.64mag in g and 0.54mag in u (see Table 2). Nevertheless we can still make approximate checks of these brighter than usual WHDF ATLAS mag limits by comparison to deeper S82 data.

So in Fig. 13 we now show in the top panel the comparison between S82 model magnitudes and ATLAS aperture

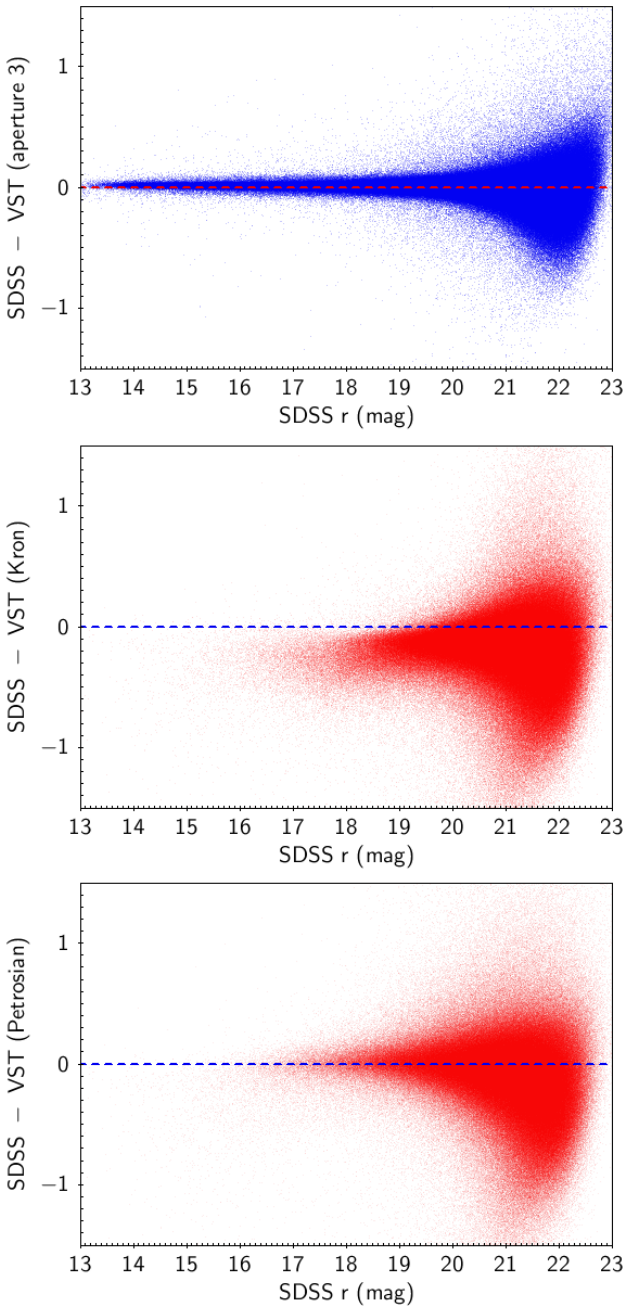

Figure 12. SDSS NGC overlap comparisons of ATLAS (APASS nightly) aperture (corrected to total), Kron and Petrosian AB magnitudes (corrected for colour terms as in Section 3.2) for stars (blue) and galaxies (red) with SDSS model magnitudes in both cases. No corrections to total magnitudes have been applied to the Kron and Petrosian magnitudes.

3 magnitudes for point sources. Again the relation is linear with a low dispersion of ±0.15mag at the 5σ WHDF ATLAS limit of $r = 22.46$ from Table 2. Indeed, ATLAS aperture magnitudes in all bands show good agreement with the S82 magnitudes to their respective 5σ limits from Table 2, confirming that the accuracy of these limits for point sources (see `http://astro.dur.ac.uk/Cosmology/vstatlas/tests`). The middle and bottom panels show the comparison between S82 model magnitudes and ATLAS

Band	u	g	r	i	z
Exposure	2 × 60s	2 × 50s	2 × 45s	2 × 45s	2 × 45s
Airmass	1.52	1.46	1.16	1.14	1.13
Seeing	1.″27	1.″36	1.″04	0.″99	1.″06
ATLAS Seeing	1.″02	0.″95	0.″90	0.″81	0.″84
Mag Lim	21.45	22.50	22.46	21.85	20.65
ATLAS Mag Lim	21.99	23.14	22.67	21.99	20.87
Sky Brightness	21.56	21.64	20.77	19.96	18.80
ATLAS Sky Bri	22.34	21.90	20.92	19.78	18.85

Table 2. ATLAS WHDF field seeing, 5σ point source magnitude limits and sky brightnesses, compared to ATLAS median parameters from Table 1. All magnitudes are quoted in the AB system.

Petrosian/Kron magnitudes now for SDSS galaxies. Both Petrosian and Kron magnitudes are reasonably linear but Petrosian appears to have a higher dispersion at $r \approx 21.5$ of ±0.2mag as opposed to ±0.15mag for Kron. On this basis the preferred ATLAS magnitude for galaxy photometry again appears to be Kron magnitudes.

4 ZERO-POINT COMPARISONS WITH APASS AND SDSS

4.1 APASS v ATLAS

We now move away from checks of the linearity of ATLAS photometry to address in more detail the question of the consistency of the ATLAS zeropoint calibration as discussed in Section 2.5 over wider areas of the survey. Maps of ESO ATLAS-APASS residuals in a ≈ 300 deg^2 area centred on RA≈ 23h, Dec≈ −30deg are shown in Fig. 14. The ATLAS data is calibrated from the ESO standards as used for the DR1 data release. The offsets in u are obtained by extrapolating to u from APASS B, V and the z offsets are from interpolating APASS r and i measurements. Offsets are seen that are clearly due to ATLAS/ESO calibration issues (generally in blocks of ∼ 17 × 1deg, corresponding to a single concatenation of tiles). Clearly some within field residuals are seen, particularly in i (and z), that do not show any ATLAS characteristics and we believe that these may be due to problems in the APASS i-band (and its extrapolation to z). The distribution of APASS-ATLAS (tile-by-tile) residuals for *ugriz* over a larger area is shown in Fig. 7 and the standard deviations are ±0.^{m}060 (u), ±0.^{m}060 (g), ±0.^{m}045 (r), ±0.^{m}038 (i), ±0.^{m}080 (z).

4.2 ATLAS-SDSS Equatorial comparison

Figs. 15-19 show the residuals between the SDSS data for stars in the NGC overlap area at 10h<RA<15h30 and −3.5 <Dec< −2deg assuming, in turn, the ESO calibration and the APASS nightly calibration for ATLAS. The SDSS magnitude ranges used are $14 < u < 20$, $15 < g < 20$, $15 < r < 20$, $14 < i < 19$ and $13.5 < z < 18.5$. The standard SDSS calibration was used here for simplicity, rather than the uber-calibration of Padmanabhan et al. (2008). As with the APASS comparison in Section 4.1, the ESO calibration clearly shows ±0.^{m}05 offsets on the scale of single concatenations. These are effectively removed by using the

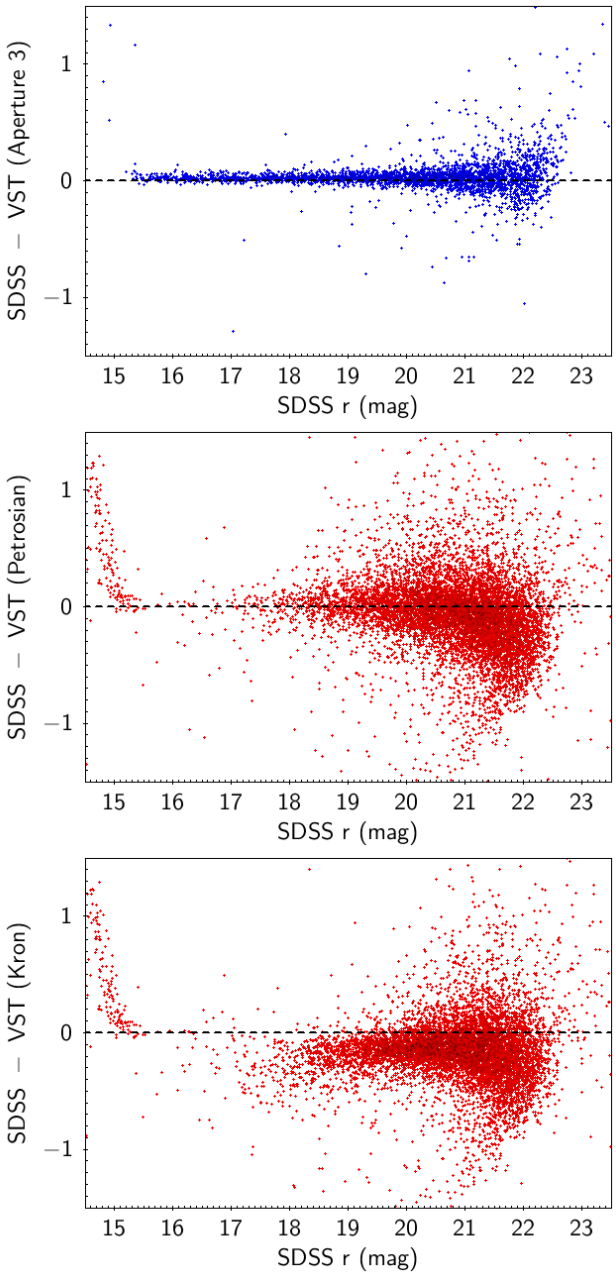

Figure 13. (top) SDSS Stripe 82 model magnitude-ATLAS aperture magnitude r-band comparison in the WHDF field for stars (blue). (middle) Same comparison now based on ATLAS Petrosian magnitudes for galaxies (red). (bottom) Same comparison now based on ATLAS Kron magnitudes for galaxies (red). In the two lower panels, saturation in S82 magnitudes of mis-classified stars causes the non-linearity at $r < 15.5$.

APASS nightly calibration. The ESO calibration also has larger residuals with clear VST nightly correlations. Some nights have no useable ESO standards and on these a long term average default value is used, perhaps explaining some of the stripes. However, even the APASS nightly calibration still has occasional issues with individual fields as can be seen in the z band image. Also, we already noted that the APASS i (and z) band photometry still has some issue from the ATLAS-APASS comparison above.

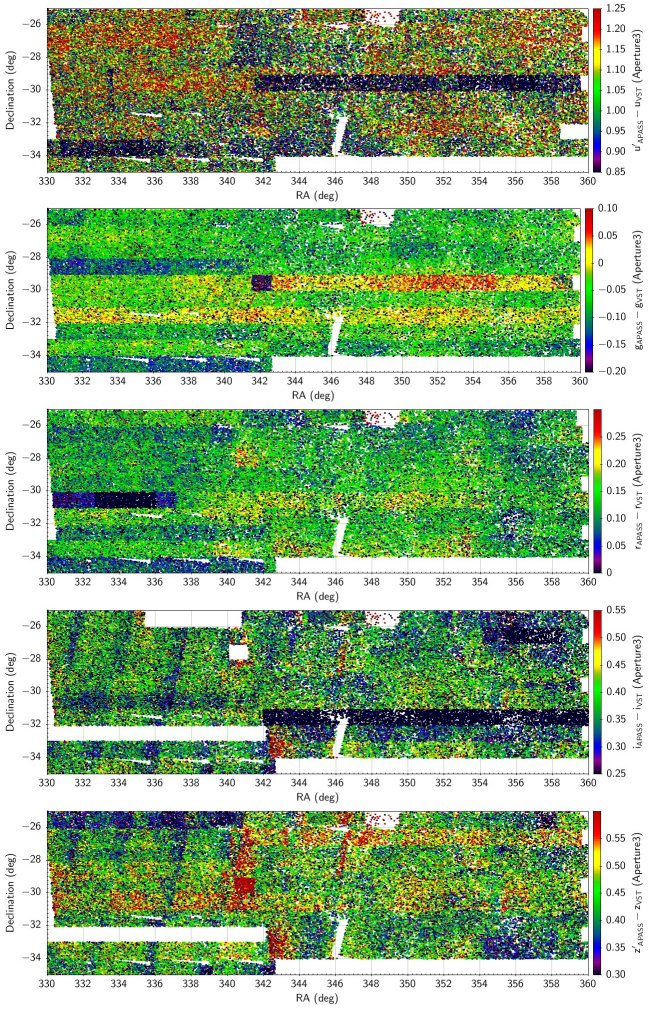

Figure 14. From top to bottom, APASS-ESO ATLAS comparisons in u (blue), g (green), r (red), i (purple), z (grey). APASS mags are in AB and ATLAS in Vega. These are for ATLAS stacks of ESO A,B grade tiles.

The distributions of SDSS-ATLAS residuals for individual stars in *ugriz* for ESO and APASS calibrations are compared in Fig. 20. Generally the APASS nightly calibrated data gives the smallest residuals with SDSS. The ESO calibration and the APASS individual fields calibration (not shown) appear to give larger residuals, in the latter case presumably due to statistical errors with the calibration based on fewer APASS stars. The ATLAS APASS nightly-SDSS mag standard deviations, measured on a tile-by-tile basis to reduce the effect of individual star random errors, are ±0.035, ±0.013, ±0.013, ±0.012 and ±0.055 mag in *ugriz*, in most bands a significant improvement over the ESO ATLAS - SDSS comparison (±0.045, ±0.027, ±0.037, ±0.035 and ±0.073 in *ugriz*). These standard deviations were measured on the basis of 183 tiles in *griz* and 112 tiles in u. In both cases, the z band result is affected by the presence of a single tile whose tile average is 0.66mag offset from the mean. Nevertheless in all bands the improvement gained from the APASS nightly calibration is clear.

Ultimately, for the final release, we shall calibrate ATLAS globally by incorporating the information from the 2′

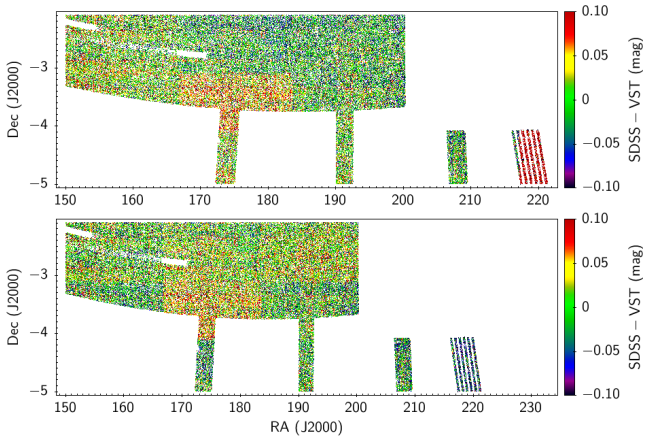

Figure 15. SDSS-ATLAS comparison in u with ATLAS/ESO-SDSS (top) and ATLAS/APASS nightly-SDSS (bottom). Aperture 3 mags are used for ATLAS and PSF magnitudes for SDSS.

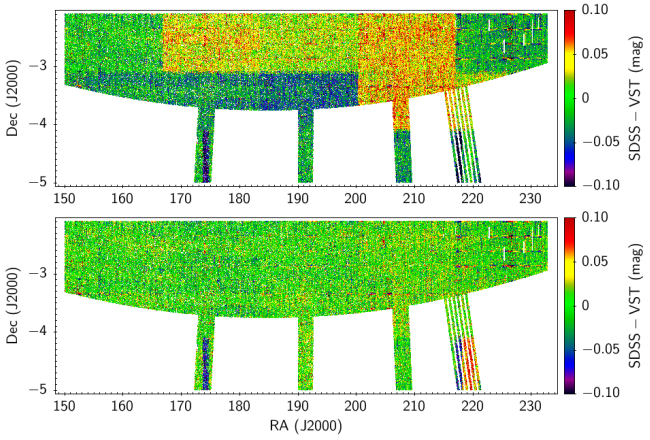

Figure 17. SDSS-ATLAS comparison in r with ATLAS/ESO-SDSS (top) and ATLAS/APASS nightly-SDSS (bottom). Aperture 3 mags are used for ATLAS and PSF magnitudes for SDSS.

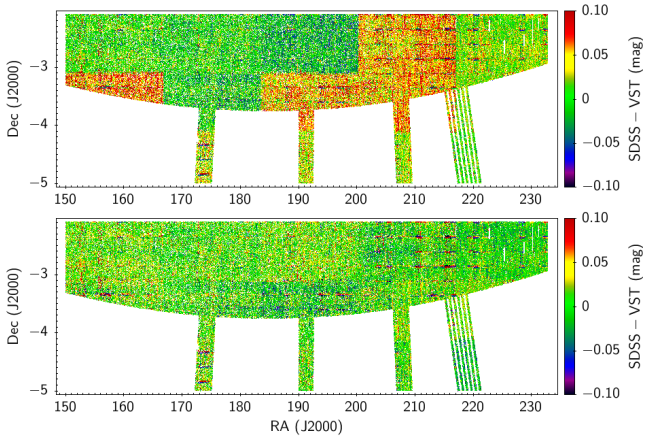

Figure 16. SDSS-ATLAS comparison in g with ATLAS/ESO-SDSS (top) and ATLAS/APASS nightly-SDSS (bottom). Aperture 3 mags are used for ATLAS and PSF magnitudes for SDSS.

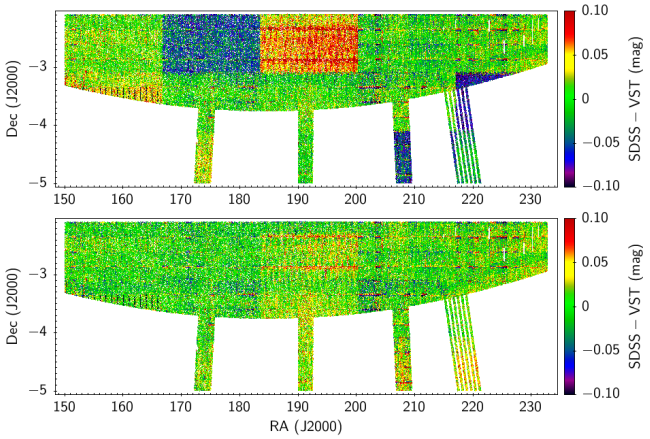

Figure 18. SDSS-ATLAS comparison in i with ATLAS/ESO-SDSS (top) and ATLAS/APASS nightly-SDSS (bottom). Aperture 3 mags are used for ATLAS and PSF magnitudes for SDSS.

overlaps in the RA and Dec directions on each field (Findlay et al. 2014b in prep.)

4.3 Star-galaxy separation comparisons

We now use the same NGC SDSS DR9 overlap area to compare ATLAS star-galaxy separation with that of SDSS. The results are shown in Fig. 21. Comparing top left and top right panels in the ATLAS Aper3-Petrosian : g magnitude star-galaxy separation plane, we see that the ATLAS star-galaxy separation statistic has included some SDSS stars just above the stellar loci shown in the lower panels. These misclassified ATLAS stars have come from areas frequently coinciding with interchip gaps as can be seen in the upper panel of Fig. 22. The problem arises when the image quality varies slightly between the 2 sub-exposures and so the stellar locus is offset in the interchip areas when there is only one sub-exposure contributing to the image. Depending on the direction of the shift, this can result in stars being classified as galaxies. This problem will clearly be present in the ATLAS DR1 data. However, it is easy to fix this problem by

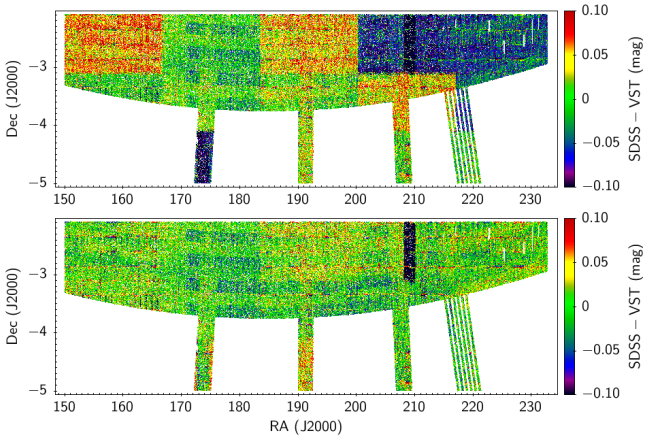

Figure 19. SDSS-ATLAS comparison in z with ATLAS/ESO-SDSS (top) and ATLAS/APASS nightly-SDSS (bottom). Aperture 3 mags are used for ATLAS and PSF magnitudes for SDSS.

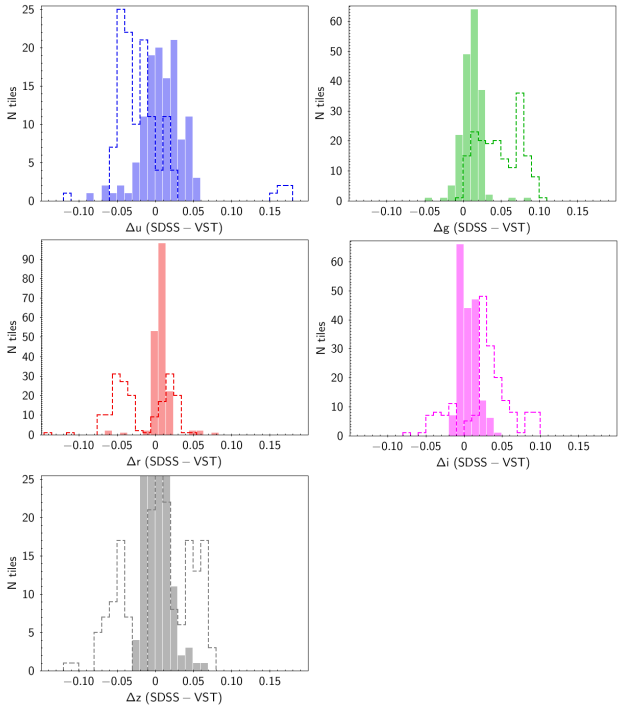

Figure 20. SDSS - ATLAS magnitude residuals for point sources in the SDSS overlap area. The dashed histograms refer to ATLAS data with ESO zeropoints. The solid histograms refer to ATLAS data with APASS nightly zeropoints. The magnitude ranges used are $14 < u < 20$, $15 < g < 20$, $15 < r < 20$, $14 < i < 19$ and $13.5 < z < 18.5$.

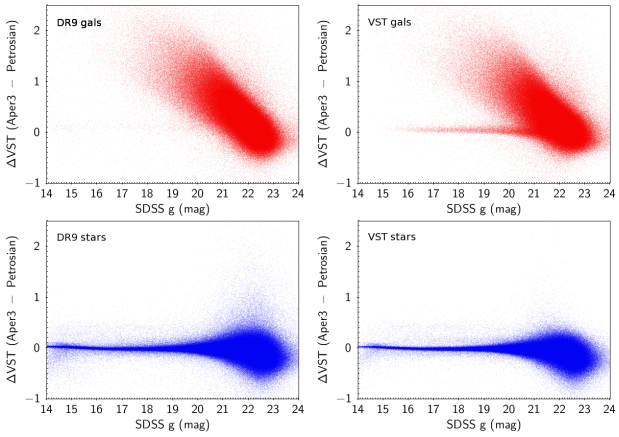

Figure 21. Star-galaxy separation comparison. *Upper*: galaxies (red) *Lower*: stars (blue). ATLAS stars mis-classified as galaxies according to SDSS in the top right panel are due to problems in partially covered interchip gaps.

plotting Δ VST (Aper$_3$-Petrosian) versus VST Petrosian for ATLAS classified galaxies and then remove the misclassified stars by a magnitude independent cut. This has the effect of cleaning up the mis-classified stars as shown in the lower panel of Fig. 22.

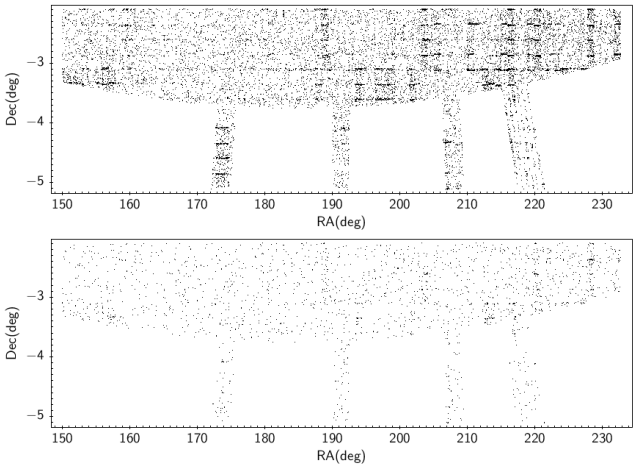

Figure 22. *Upper* Map showing ATLAS classified galaxies which are stars according to SDSS, down to $g \approx 20.5$. These are found particularly in areas corresponding to interchip gaps. *Lower*: Same as above except the additional star-galaxy separation method described in Section 4.3 has now been applied to the ATLAS galaxies.

5 GALAXY AND STAR NUMBER COUNTS

Adopting the corrected star - galaxy classifier, we next calculate the galaxy (and star) counts from 250deg^2 in the $-40 < Dec < -25$ deg range in the SGC which includes the SGP. Previously 2MASS counts have suggested evidence for a local underdensity in the SGP region. Here we simply focus on the counts to use their turnover to indicate the rough completeness limits of the survey. In Fig. 23 we compare these to a variety of previous galaxy counts compiled by Metcalfe et al. (2001). 2MASS counts suggest evidence for a local underdensity in the SGP region (Whitbourn & Shanks 2014) but a fuller investigation of this issue using ATLAS data in a bigger area will be presented by Mackenzie et al (2014, in prep.). We see that the galaxy counts agree very well in most bands with other authors until the counts turn over due to incompleteness at faint magnitudes. This happens at AB mags $u \approx 20$, $g \approx 22.5$, $r \approx 22$, $i \approx 21$ and $z \approx 20$. These are in reasonable agreement with the Mag Lim (gal) 5σ limits for ATLAS given in Table 1. Star counts turn over at about the same limits but this is more dictated by the star-galaxy separation algorithm and is less related to more fundamental signal-to-noise considerations.

6 ACCESS TO ATLAS DATA

The ESO Science Archive provides a repository for data products released by the ESO Public Survey teams. Images and catalogues from ATLAS Data Release 1 can be retrieved from `http://archive.eso.org/wdb/wdb/adp/phase3_main/form?phase3_collection=ATLAS&release_tag=1`.

ATLAS data are also available through the OmegaCAM Science Archive (OSA, `http://osa.roe.ac.uk`), curated by the Wide-Field Astronomy Unit (WFAU) at the University of Edinburgh. Similar in design to the science archives developed by WFAU for sky survey data from UKIRT/WFCAM (Hambly et al. 2008) and VISTA (Cross et al. 2012), the OSA provides a range of access methods to both image and

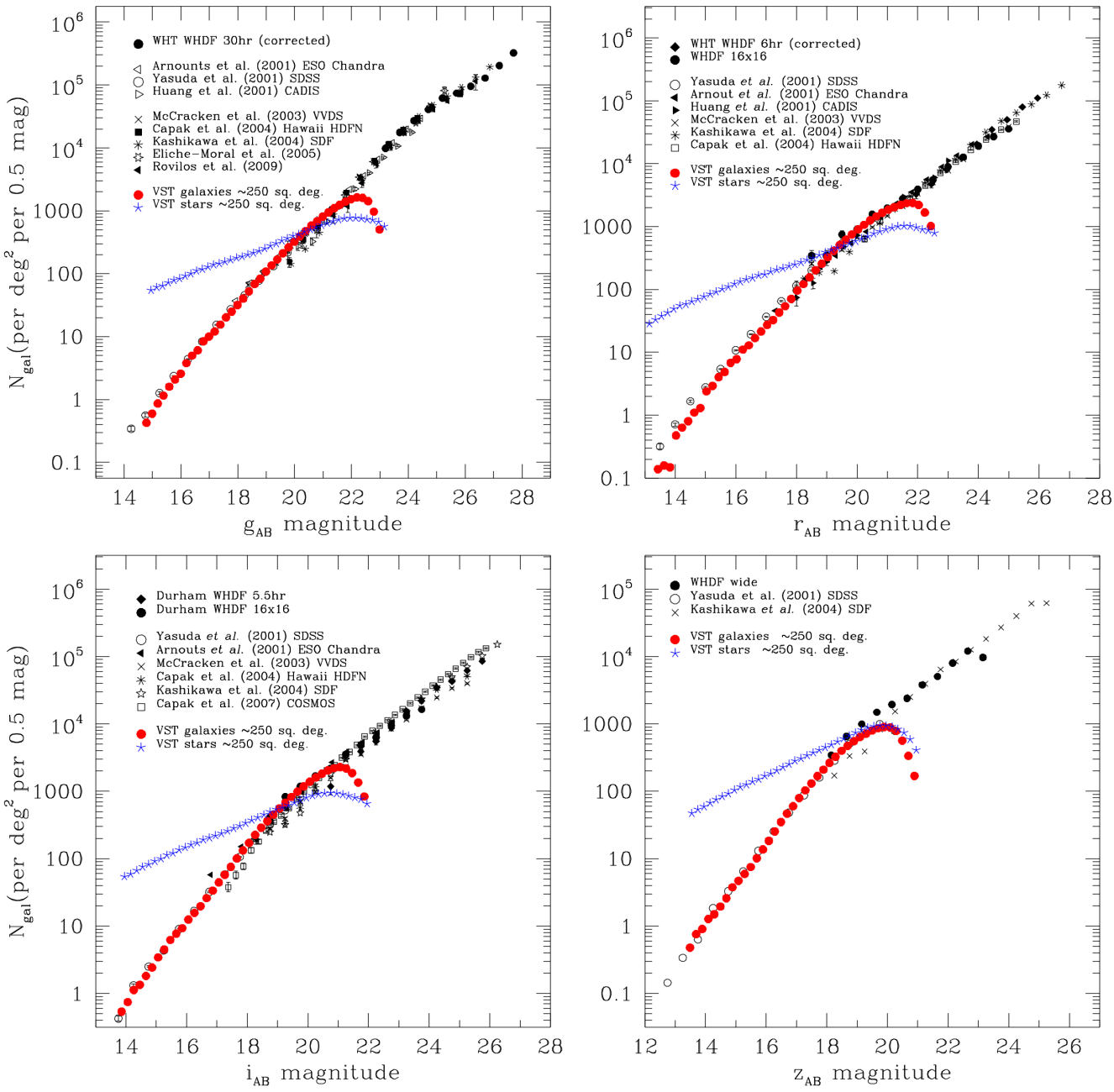

Figure 23. ATLAS galaxy and star counts compared to SDSS and other galaxy counts. Both stars and galaxies are measured in Kron magnitudes, brightened by $0.^m15$ to take them to total.

catalogue data products. It stores ATLAS catalogue data and image metadata in a relational database management system, which can be queried through the OSA web interface or using the Virtual Observatory (VO) Table Access Protocol (Dowler, Rixon, & Tody 2011). Query results can be viewed within the OSA web interface or sent directly from it to VO-compliant desktop tools like Aladin (Bonnarel et al. 2000) and TOPCAT (Taylor 2005), using the Simple Application Message Protocol (Taylor et al. 2012) standard. The OSA also integrates ATLAS catalogue data with a number of sky survey datasets, including SDSS, 2MASS, VHS and WISE, and provides the ATLAS consortium with access to proprietary data, as well as supporting use of ATLAS public data releases by the wider astronomical community.

7 CONCLUSIONS

We have described the basic characteristics of VST ATLAS. We find it meets its basic specification of comprising a 'Southern Sloan'. This applies both to the median 5σ magnitude limits for point sources which are at least as deep as SDSS and to the median sky brightnesses which are comparable to SDSS. But in terms of its spatial resolution, the

ATLAS survey presents essentially sub-arcsecond $0.''8-1.''0$ median seeing compared to the $1.''2-1.''5$ median imaging of SDSS.

We have derived the colour equations relating ATLAS stellar photometry to SDSS photometry. We find there are small but non-negligible colour terms, particularly in grz.

We have demonstrated the linearity of the ATLAS photometry by comparison in the 120deg^2 NGC overlap area with SDSS. We recommend that $1''$ radius (aperture 3) apertures are used for stellar photometry. For galaxies, ATLAS Kron magnitudes seem to give the most linear relations with SDSS model magnitudes. The same conclusions are found by comparing ATLAS and Stripe 82 photometry in the WHDF field. Here we found that the rms dispersions reached ±0.05 mag for stars at $r < 22$ and ±0.15mag for Kron galaxy magnitudes at $r < 21.5$mag

The current zeropoints assumed for $ugriz$ come from APASS stellar photometry applied nightly and appear good to $\approx \pm0.02$mag by comparison with SDSS data in overlap areas. We have investigated how area dependent these zeropoints are in the SDSS overlap area and find there are still small areas with residual errors. In the final global calibration we shall use the $2'$ overlaps between tiles to reduce these errors.

We have tested the ATLAS star-galaxy separation by comparison with SDSS in the overlap areas and we found that 10% galaxies were misclassified as stars. We also found that 15% stars were misclassified as galaxies and that this higher rate was due to problems occurring in interchip gaps where only one sub-exposure was available. However, the problem is easily cured by using a more conservative star-galaxy separation line particularly at bright magnitudes.

Finally we also presented galaxy and star number counts in a 250deg^2 area at the SGP and found where they turned over to define effective completeness limits. The galaxy counts turn over about at about our quoted 5σ mag limits for galaxies. Star counts turn over at about the same limits but this is mainly dictated by the star-galaxy separation algorithm.

We conclude that the VST ATLAS is ready for scientific analysis. Currently the survey is 75% complete and it should be 100% complete by the end of 2015.

ACKNOWLEDGEMENTS

We are grateful to European Southern Observatory (ESO) and their associated service time VLT Survey Telescope observers for carrying out the ATLAS observations. We are indebted to the Cambridge Astronomical Surveys Unit (CASU) for reducing the ATLAS images and producing catalogues. We also acknowledge the work of the Wide Field Astronomy Unit (WFAU) at Edinburgh for archiving the ATLAS data. We also acknowledge use of publicly available SDSS data. This research has also made use of the APASS database, located at the AAVSO web site. Funding for APASS has been provided by the Robert Martin Ayers Sciences Fund.

REFERENCES

Belokurov V., Irwin M. J., Koposov S. E., Evans N. W., Gonzalez-Solares E., Metcalfe N., Shanks T., 2014, MNRAS, 441, 2124
Bonnarel F., et al., 2000, A&AS, 143, 33
Bovy J., et al., 2012, ApJ, 749, 41
Bramich D. M., Freudling W., 2012, MNRAS, 424, 1584
Cross N. J. G., et al., 2012, A&A, 548, A119
de Jong J. T. A., et al., 2013, Msngr, 154, 44
Dowler P., Rixon G., Tody D., 2011, arXiv, arXiv:1110.0497
Edge A., Sutherland W., Kuijken K., Driver S., McMahon R., Eales S., Emerson J. P., 2013, Msngr, 154, 32
Goto T., et al., 2002, PASJ, 54, 515
Hambly N. C., et al., 2008, MNRAS, 384, 637
Irwin M. J., et al., 2004, SPIE, 5493, 411
Keenan R. C., Barger A. J., Cowie L. L., 2013, ApJ, 775, 62
Koposov S. E., Irwin M., Belokurov V., Gonzalez-Solares E., Yoldas A. K., Lewis J., Metcalfe N., Shanks T., 2014, MNRAS, 442, L85
Kuijken K. et al, 2011, Msngr, 146, 8
McMahon R. G., Banerji M., Gonzalez E., Koposov S. E., Bejar V. J., Lodieu N., Rebolo R., the VHS Collaboration, 2013, Msngr, 154, 35
Merloni A., et al., 2012, arXiv, arXiv:1209.3114
Metcalfe N., Shanks T., Campos A., McCracken H. J., Fong R., 2001, MNRAS, 323, 795
Metcalfe N., Shanks T., Weilbacher P. M., McCracken H. J., Fong R., Thompson D., 2006, MNRAS, 370, 1257
Mountrichas G., Shanks T., 2007, MNRAS, 380, 113
Padmanabhan N., et al., 2008, ApJ, 674, 1217
Sawangwit U., Shanks T., Cannon R. D., Croom S. M., Ross N. P., Wake D. A., 2010, MNRAS, 402, 2228
Schipani P., et al., 2012, SPIE, 8444, 8441C
Shanks T., et al., 2013, Msngr, 154, 38
Stoughton C., et al., 2002, AJ, 123, 485
Taylor M. B., 2005, ASPC, 347, 29
Taylor M., et al., 2012, ivoa.spec, 1104
Whitbourn J. R., Shanks T., Sawangwit U., 2014, MNRAS, 437, 622
Whitbourn J. R., Shanks T., 2014, MNRAS, 437, 2146
Wright E. L., et al., 2010, AJ, 140, 1868